NSS

Neutrosophic Sets and Systems, Vol. 99, 2026

University of New Mexico

Iterative Neutrosophic Refinement for Reliable Tumor Segmentation in Brain MRI Images

Sofia Jennifer J[1], Kalaivani C [2] and Saraswathi S[3]

[1]Department of Information Technology, Sri Sivasubramaniya Nadar College of Engineering, Chennai 603 110, India; sofiajenniferj@ssn.edu.in

[2]Department of Mathematics, Sri Sivasubramaniya Nadar College of Engineering, Chennai 603 110, India; kalaivanic@ssn.edu.in

[3]Department of Computer Science and Engineering, Sri Sivasubramaniya Nadar College of Engineering, Chennai 603 110, India; saraswathis@ssn.edu.in

*Correspondence: kalaivanic@ssn.edu.in;

Abstract. Accurate segmentation of brain tumors in MRI scans is important for diagnosis and treatment, but noise, overlapping tissues, low contrast, and unclear boundaries make it difficult for traditional image processing methods. Our idea is to present a robust method for brain tumor segmentation using Refined Neutrosophic Set (NRS). This approach builds on the traditional neutrosophic framework by breaking down truth, indeterminacy, and falsity into multiple subcomponents for better handling of uncertainty . The input MRI images is transformed into the neutrosophic refined set domain, and then iterative refinement of truth and indeterminacy is applied. This method effectively handles uncertainty, reduces ambiguity, and produces clearer, more accurate tumor boundaries. Experimental results on benchmark MRI datasets demonstrate that the NRS-based method achieves higher Dice similarity scores and lower Hausdroff distance.

Keywords: Brain tumor, Refined neutrosophic sets, Tumor segmentation, Medical imaging.

1. Introduction

Brain tumors are abnormal growths of cells within the brain or central nervous system (CNS) that can be either benign or malignant [3]. Early and accurate detection of brain tumors play a vital role, as timely treatments increase the chances of survival.

Traditional methods for detecting brain tumors include clinical evaluation, neurological examinations, and imaging techniques such as Magnetic Resonance Imaging (MRI) and Computed Tomography (CT) scans [15]. These methods are time-consuming, prone to inter-observer variability, and heavily reliant on expert interpretation. Image processing methods are used on MRI or CT scans and usually involve steps like preprocessing, feature extraction, and segmentation. However, these medical images often have problems such as noise, unclear boundaries, and low contrast, which make them difficult to interpret accurately. Traditional techniques, and even some machine learning methods, fail to deal with this uncertainty, especially when tissues overlap or artifacts are present in the scans. As a result, mistakes can occur in important tasks like segmentation, classification, and tumor detection.

Neutrosophic theory [11], introduced by Florentin Smarandache, designed a mathematical framework to handle truth (T), indeterminacy (I), and falsity (F) simultaneously. Fuzzy approaches usually focus on truth degree whereas neutrosophic sets focuses on uncertainty and ambiguity, thus making it suitable for medical images as it is prone to noise, low resolution, and partial volume effects. The basic neutrosophic approach (T, I , F) is not sufficient to fully capture the subtle variations and multiple layers of uncertainty present in medical imaging data. This limitation reduces the accuracy and reliability of tumor detection and diagnosis.

To handle this issue, the proposed work focuses on applying Neutrosophic Refined Sets (NRS) an extension of classical neutrosophic framework by dividing truth, indeterminacy, and falsity into smaller parts, giving a more detailed and flexible way to represent uncertainty. This refinement improves pre-processing, segmentation, and tumor detection, leading to more accurate boundary identification, reduced false positives/negatives, and enhanced diagnostic performance. Specifically, the proposed work aims to apply NRS to brain tumor segmentation, demonstrating its effectiveness in producing clearer images and supporting better medical decision-making.

2. **Related Works**

Many researchers have been done on localizing tumors in medical images to accurate tumor localization as it is critical for diagnosis and treatments. Various techniques, ranging from traditional image processing methods to advanced machine learning and deep learning approaches, have been explored to identify tumor regions. Despite significant progress, challenges such as noise, low contrast, overlapping tissues, and ambiguous boundaries is still open for research.

Khan et al. [4] proposed a method to grade brain tumors by first using thresholding to separate the tumor, then measuring features like size, shape, and density. These features were used with the Partial tree algorithm (PART) for classification. Sharif et al. [10] improved the traditional thresholding approach using particle swarm optimization (PSO) to better separate tumor and healthy tissues. They extracted local binary patterns (LBP) along with deep features from a capsule network, selected the most useful ones with a genetic algorithm (GA), and classified tumor grades using artificial neural network (ANN), a support vector machine (SVM), and an ensemble of linear discriminant analysis (LDA) models. Oliva et al. [1] used an adaptive LSHADE metaheuristic with minimum cross-entropy as the fitness function to optimize thresholding for brain tissue segmentation in MR images. Similarly, Renugambal et al. [9] introduced a hybrid method combining Otsu with a water cycle–moth-flame optimization (WCMFO) algorithm to improve segmentation on T2-weighted MR images, though the model faced limitations in handling several parameters.

Guo et al. [2] proposed a neutrosophic transformation of MRI images followed by alpha-mean clustering lead to good segmentation performance. Majumder et al. [7] combined neutrosophic set theory with morphological operations to refine tumor edges, effectively reducing false positives in heterogeneous tumor regions. Kundu et al. [6] integrated neutrosophic preprocessing with Fuzzy C-Means (FCM) clustering to enhance tumor extraction in low-contrast MRI images, demonstrating the robustness of neutrosophic-based methods under challenging imaging conditions.

Several studies have demonstrated the effectiveness of Neutrosophic Refined Sets (NRS) in brain tumor segmentation. Mohamed et al. [8] applied NRS to MRI images by refining truth and indeterminacy maps, which reduced false detections at tumor boundaries and improved Dice scores compared to classical Fuzzy C-Means (FCM). Similarly, Khan et al. [5] employed NRS-based clustering combined with morphological operations to segment glioma regions, showing that the approach is robust even in low-contrast images. These studies highlight the potential of NRS in enhancing segmentation accuracy and handling uncertainty in medical imaging.

Our proposed work focuses on brain tumor detection and segmentation using a Neutrosophic Refined Set (NRS) based approach. MRI images are first converted into the neutrosophic refined set domain to handle uncertainty, indeterminacy, and noise. Multiple truth and indeterminacy components are refined to enhance tumor boundary definition. Segmentation is performed using a clustering to extract tumor regions.

3. Proposed Work

This study proposes an automated framework for brain tumor detection and localization using MRI images and Neutrosophic Reconstructed Sets (NRS). The workflow, illustrated in Figure 1, comprises the following stages: (i) Input MRI Image Acquisition, (ii) NRS Feature Extraction, (iii) Initial Truth Map Refinement, (iv) Iterative Truth Map Refinement, (v) Final NRS-Based Image Reconstruction, and (vi) Tumor Localization through Segmentation.

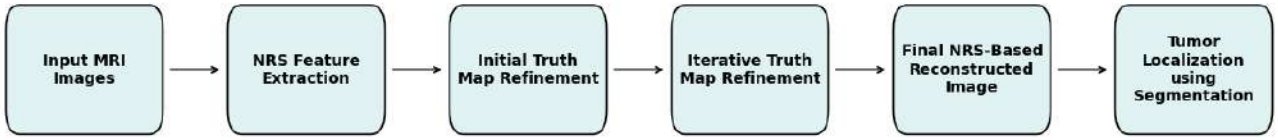

FIGURE 1. NRS-Based MRI Reconstruction and Tumor Localization

3.1. *Input MRI Image Acquisition*

Magnetic resonance imaging (MRI) scans of the brain, containing tumor-affected regions, are webcrawled from open-source datasets. These images when acquired contains noise due to acquisition conditions, patient movement, or scanner limitations.

3.2. *NRS Feature Extraction*

As per definition a neutrosophic refined set generalizes the neutrosophic set by allowing each of the three membership components such as Truth (T), Indeterminacy (I) and Falsity (F) to be refined into one or more sub-memberships.

To transform an image $I(x, y)$ into the Neutrosophic Refined Set (NRS) domain, each pixel is decomposed into multiple refined components based on different sources of information and uncertainty [12]. Formally, the NRS representation of a pixel (x, y) is given as

$$\begin{aligned} NRS(x,y) = \Big(& \{T_1(x,y), T_2(x,y), \ldots, T_p(x,y)\}, \\ & \{I_1(x,y), I_2(x,y), \ldots, I_q(x,y)\}, \\ & \{F_1(x,y), F_2(x,y), \ldots, F_r(x,y)\} \Big), \end{aligned} \tag{1}$$

where $T_i(x, y)$, $I_j(x, y)$, and $F_k(x, y)$ denote the truth, indeterminacy, and falsity components, respectively.

For the present study, we select $p = 2$ truth components, $q = 2$ indeterminacy components, and $r = 1$ falsity component, with each sub-value constrained to the interval $[0, 1]$.

T_1: Truth from Intensity Closeness (Uniformity)

This component represents the truth degree derived from intensity closeness, reflecting the uniformity of pixel values within a suspected tumor region

$$T_1(x,y) \;=\; 1 - \frac{\left|I(x,y) - \mu_{W_{xy}}\right|}{I_{\max} - I_{\min}}, \tag{2}$$

where $\mu_{W_{xy}}$ is the mean intensity in the local window centered at (x,y), and $I_{\max}, I_{\min}$ are the maximum and minimum intensity values in the image.

T_2: Truth from Gradient (Edges)

T_2 captures truth from gradient information, highlighting edges and structural boundaries.

$$T_2(x,y) \;=\; 1 - \frac{\|\nabla I(x,y)\|}{\|\nabla I\|_{\max}}, \tag{3}$$

where $\|\nabla I(x,y)\|$ is the gradient magnitude at pixel (x,y), and $\|\nabla I\|_{\max}$ is the maximum gradient magnitude in the entire image.

I_1: Indeterminacy from Noise Level

This component measures local variance, indicating uncertainty due to heterogeneous intensity patterns.

$$I_1(x,y) \;=\; \frac{\sigma_{W_{xy}}}{\sigma_{\max}}, \tag{4}$$

where $\sigma_{W_{xy}}$ is the standard deviation of intensities within the local window centered at (x,y), and $\sigma_{\max}$ is the maximum standard deviation observed in the image.

I_2: Indeterminacy from Contrast Ambiguity

This component measures local entropy, representing uncertainty arising from textural complexity or disorder in the neighborhood.

$$I_2(x,y) = \frac{H(W_{xy})}{H_{\max}} \tag{5}$$

where the local entropy $H(W_{xy})$ is defined as

$$H(W_{xy}) = -\sum_i p_i \log_2 p_i, \tag{6}$$

with p_i denoting the probability of intensity level i in the window W_{xy}, and $H_{\max}$ representing the maximum possible entropy.

F_1: Falsity (complement of truth evidence) The falsity component $F_1(x, y)$ is designed to represent how much a pixel belongs to the non-tumor or background region. It is defined as the complement of the truth information, given by

$$F_1(x, y) = 1 - \frac{T_1(x, y) + T_2(x, y)}{2} \tag{7}$$

where $T_1(x, y)$ and $T_2(x, y)$ denote the intensity-based and gradient-based truth measures, respectively.

Figure 2 gives the decomposition of pixel evidence in MRI brain tumor analysis and Figure 3 portrays the transformation of a noisy MRI Image into NRS Components$(T_1, T_2, I_1, I_2, F_1)$.

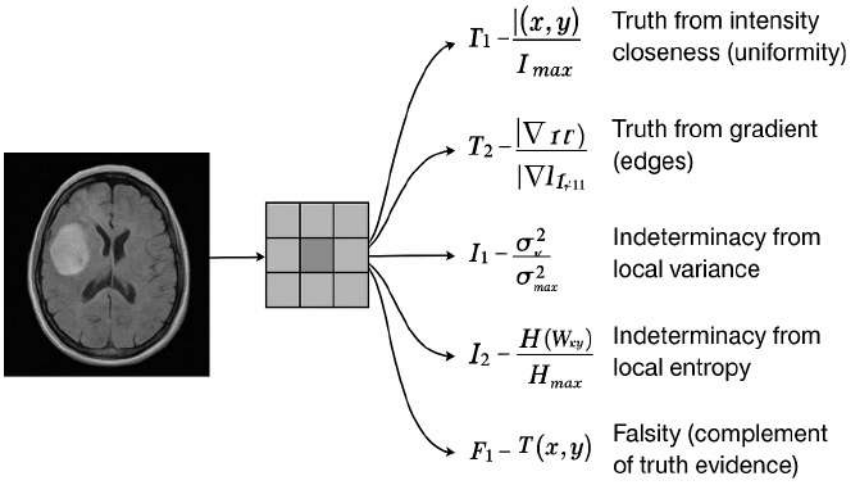

FIGURE 2. NRS decomposition of pixel evidence in MRI brain tumor analysis

3.3. *Initial Truth Map Refinement*

This step aims to improve segmentation by boosting the reliability of truth evidence while reducing the effect of uncertainty. This is achieved by adjusting the truth components T_1 and T_2 in proportion to the indeterminacy components I_1 and I_2. The refined truth values are computed as:

$$T_1' = \frac{T_1}{1 + \alpha \cdot (I_1 + I_2)}, \quad T_2' = \frac{T_2}{1 + \alpha \cdot (I_1 + I_2)} \tag{8}$$

where $\alpha > 0$ is a control parameter.

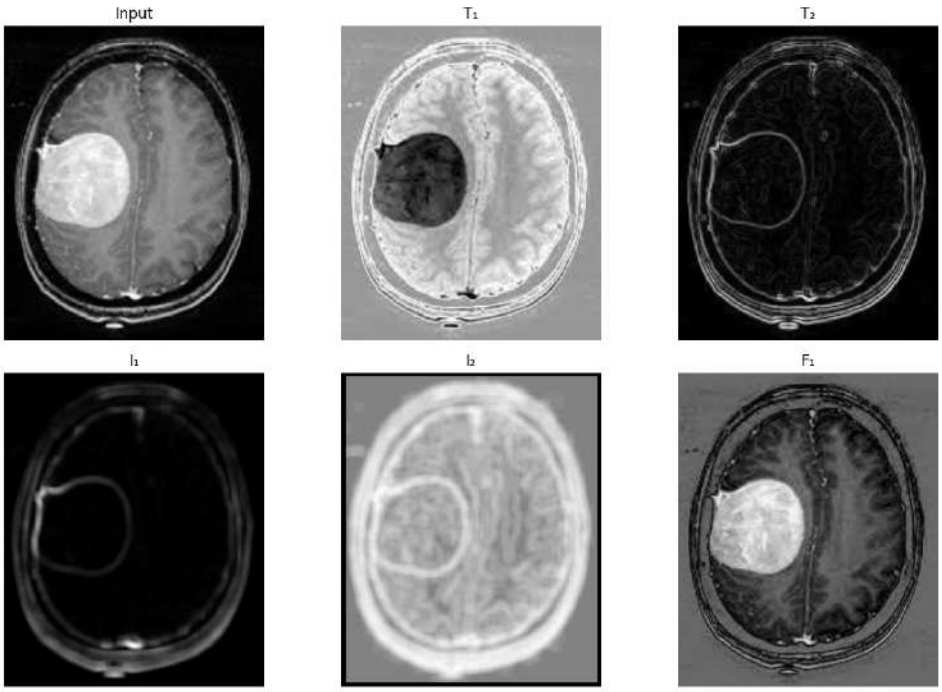

FIGURE 3. Transformation of a Noisy MRI Image into NRS Components$(T_1, T_2, I_1, I_2, F_1)$

- A larger α strongly suppresses uncertainty, reducing the influence of noisy or ambiguous pixels.
- A smaller α preserves more original truth evidence, which may help retain fine details but could include more noise.

To explicitly suppress redundancy in uncertain regions, the indeterminacy maps are reduced as follows:

$$I_1' = \frac{I_1}{1 + \beta \cdot (T_1 + T_2)}, \quad I_2' = \frac{I_2}{1 + \beta \cdot (T_1 + T_2)} \tag{9}$$

where $\beta > 0$ is a control parameter that regulates the amount of indeterminacy suppression. The proposed system works well when $\alpha = 0.9$ and $\beta = 0.9$

- Pixels where $T_1 + T_2$ is strong experience more reduction in I_1' and I_2'.
- This step enhances the contrast between reliable and uncertain regions.

This enhancement process can be interpreted as a regularization step: it penalizes pixels with high variance or entropy (i.e., uncertain regions), while giving greater weight to pixels with reliable intensity and gradient-based truth evidence. The resulting refined maps (T_1', T_2', I_1', I_2') as shown in Figure 4 are more robust, improving the accuracy of tumor segmentation in noisy MRI scans.

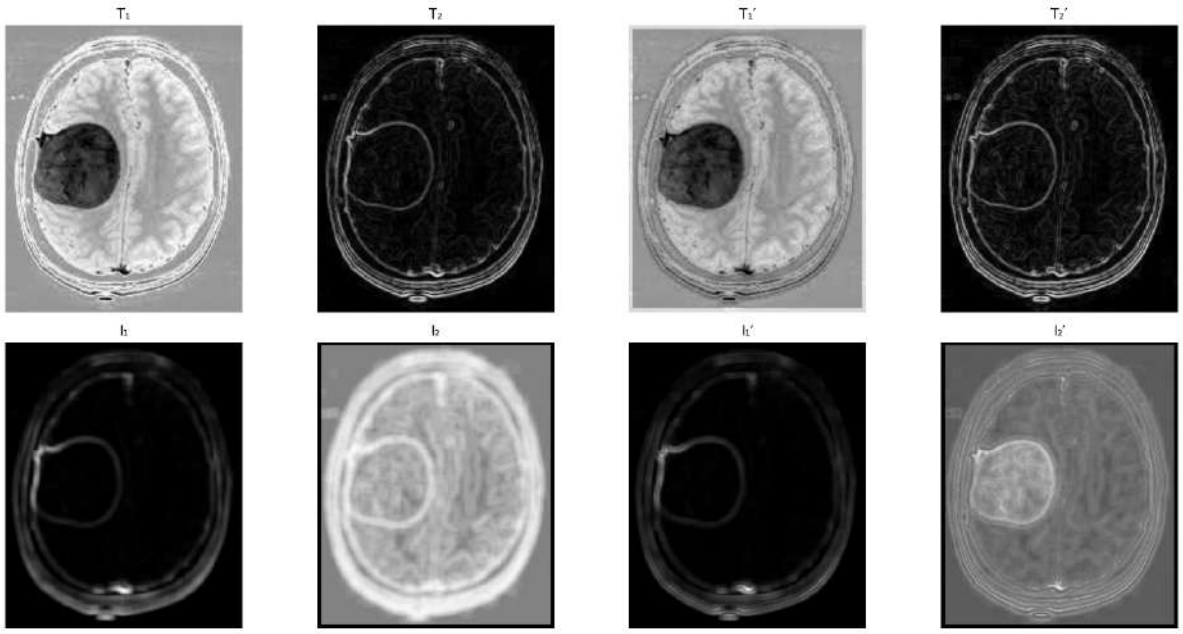

FIGURE 4. Initial Truth Map Refinement (T_1', T_2', I_1', I_2')

3.4. *Iterative Truth Map Refinement*

The iterative enhancement of NRS maps gradually refines the truth maps (T_1, T_2) while reducing indeterminacy (I_1, I_2). In the first iteration, T_1', T_2' are enhanced and I_1', I_2' are reduced. In the second iteration, the process is repeated to obtain T_1'', T_2'' and I_1'', I_2'', This makes tumors stand out more clearly from the background, removes unwanted noise, and preserves important small details. It also adapts to local variations in the image and becomes more stable over iterations, resulting in more accurate and reliable segmentation.

$$I_1'' = \frac{I_1'}{1 + \beta \cdot (T_1' + T_2')}, \quad I_2'' = \frac{I_2'}{1 + \beta \cdot (T_1' + T_2')} \tag{10}$$

$$T_1'' = \frac{T_1'}{1 + \alpha \cdot (I_1'' + I_2'')}, \quad T_2'' = \frac{T_2'}{1 + \alpha \cdot (I_1'' + I_2'')} \tag{11}$$

Here, $\alpha > 0$ and $\beta > 0$ are control parameters that regulate truth enhancement and indeterminacy suppression, respectively. After two iterations, T_1'', T_2'' are the refined truth maps, and I_1'', I_2'' are the reduced indeterminacy maps as shown in Figure 5.

3.5. *Final NRS-Based Image Reconstruction*

The reconstructed image combines the enhanced truth maps (T_1'', T_2'') into a single unified representation as shown in Figure 6 captures all reliable information from the input. It is

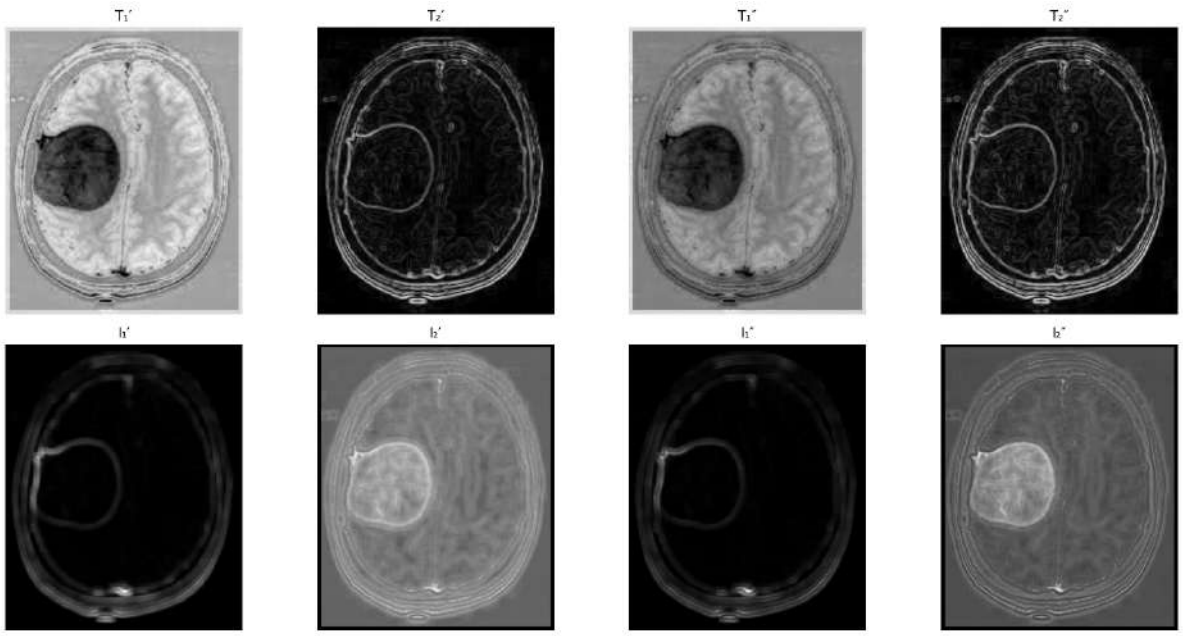

FIGURE 5. Iterative Truth Map Refinement $(T_1'', T_2'', I_1'', I_2'')$

computed as

$$R = \frac{T_1'' + T_2''}{2} \times \left(1 - \gamma \cdot (I_1'' + I_2'')\right), \tag{12}$$

where γ (values between 0.5 and 1)is a weight factor controlling the influence of uncertainty. By penalizing the residual indeterminacy (I_1'', I_2''), the reconstruction suppresses noise and ambiguous regions, resulting in a cleaner and more robust image that effectively highlights tumor regions and provides a solid basis for accurate segmentation and analysis.

3.6. *Tumor Localization through Segmentation*

Tumor localization is performed by applying k-means clustering on the reconstructed image R. In k-means, pixels are grouped into k clusters by minimizing the within-cluster variance:

$$J = \sum_{i=1}^{k} \sum_{x \in C_i} \|x - \mu_i\|^2, \tag{13}$$

where C_i is the i-th cluster, μ_i is its centroid, and x represents pixel intensities. The algorithm typically separates tumor regions from the background. After clustering, small or irrelevant clusters are removed, retaining the most significant cluster corresponding to the tumor. This approach highlights tumor regions in distinct colors as shown in Figure 7, facilitating visualization and further quantitative analysis.

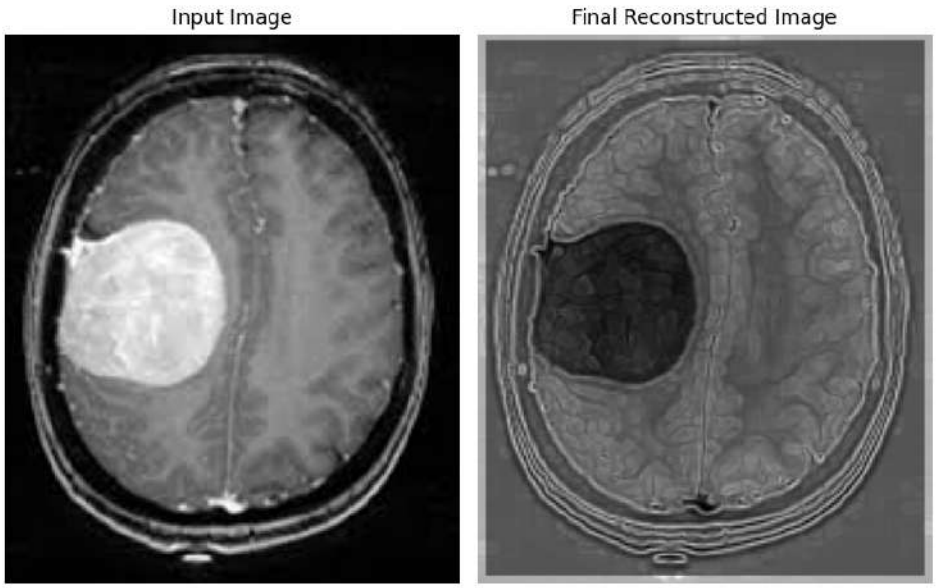

FIGURE 6. Final NRS-Based Image Reconstructio

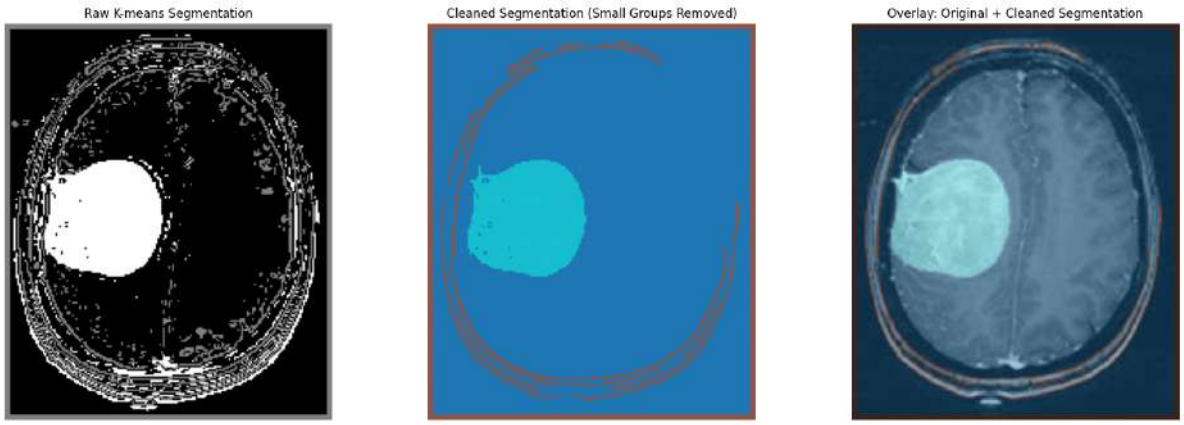

FIGURE 7. Tumor Localization through Segmentation

4. **Experimental Results and Discussion**

4.1. *Dataset*

The input images are download from the Brain MRI Images for Brain Tumor Detection dataset, hosted on Kaggle. It comprises a collection of MRI scans categorized into two classes: Tumor and No Tumor. These images are preprocessed and resized to 512x512 pixels to standardize size. Each image is accompanied by a corresponding label indicating the presence or absence of a tumor.

4.2. *Performance Metrics*

The performance metrics [14] [13] used are Dice Similarity Coefficient (DSC) and Hausdorff Distance.

Dice Similarity Coefficient (DSC):

This metric is used to evaluate the accuracy of tumour segmentation. It quantifies the overlap between the predicted segmentation mask and the actual ground truth mask by the following Equation

$$\text{DSC} = \frac{2|S_p \cap S_g|}{|S_p| + |S_g|} \tag{14}$$

where S_p represents the predicted segmentation and S_g the ground truth. The DSC values usually ranges from 0 to 1, where a value of 1 indicates perfect overlap and 0 indicates no overlap. Greater the DSC value signify that the predicted segmentation closely matches the ground truth, thus quantify its purpose of assessing the quality of tumor detection and segmentation in MRI scans.

Hausdorff Distance (HD) This metric is used to quantify the maximum distance between the boundaries of a predicted segmentation and the ground truth. Unlike Dice, it focuses on the geometric accuracy of the segmentation contours. Mathematically, for a predicted set of boundary points S_p and ground truth boundary points S_g, the Hausdorff Distance is defined as:

$$HD(S_p, S_g) = \max\left\{ \sup_{x \in S_p} \inf_{y \in S_g} d(x,y),\ \sup_{y \in S_g} \inf_{x \in S_p} d(x,y) \right\} \tag{15}$$

where $d(x, y)$ represents the Euclidean distance between points x and y. A lower HD value indicates that the predicted boundary closely follows the ground truth, while a higher value reflects larger deviations or outlier errors. This metric plays an important role in medical image analysis because precise boundary delineation is crucial for treatment planning and quantitative evaluation of tumor regions.

4.3. *Experimental Results*

Table 1 tabulates the performance of the NRS-based tumor segmentation on random five MRI cases from the dataset. The Dice scores range from 0.91 to 0.95, with an average of 0.93, indicating excellent overlap between the predicted tumor regions and the ground truth masks. Simultaneously, the Hausdorff Distances are low, ranging from 1.5 to 1.9 pixels, with an average of 1.7 pixels, reflecting precise boundary alignment and minimal deviation from

Table 1. Performance of NRS-based Tumor Segmentation on MRI Cases

Image/Patient	Dice (DSC)	Hausdorff Distance (HD, px)
Patient 1	0.92	1.8
Patient 2	0.95	1.5
Patient 3	0.93	1.7
Patient 4	0.94	1.6
Patient 5	0.91	1.9
Average	**0.93**	**1.7**

the true tumor contours. Overall, the results demonstrate that the proposed segmentation framework achieves both high accuracy in region overlap and strong geometric fidelity at the tumor boundaries.

5. Conclusion

In this work, we proposed a robust brain tumor segmentation method based on Refined Neutrosophic Set (NRS) theory with iterative truth–indeterminacy refinement. This approach effectively handles uncertainty in MRI images, improves tumor boundary detection, and reduces errors. The results demonstrate that the proposed method achieves excellent overlap with ground truth tumor regions and precise alignment of tumor boundaries, indicating both high segmentation accuracy and strong geometric fidelity. The study highlights the potential of neutrosophic refined set approaches in improving medical image analysis and supporting clinical decision-making.

Future Work will concentrate on combining NRS-based method with deep learning and apply it to different types of MRI scans for better tumor analysis.

Funding: This research received no external funding.

Conflicts of Interest: The authors declares that there is no conflict of interest regarding the publication of this paper.

References

1. Aranguren, I.; Valdivia, A.; Morales-Castaneda, B.; Oliva, D.; Elaziz, M.A.; Perez-Cisneros, M. Improving the segmentation of magnetic resonance brain images using the LSHADE optimization algorithm. Biomed. Signal Process. Control 2021, 64, 102259. https://doi.org/10.1016/j.bspc.2020.102259.
2. Guo, L.; Yu, F.; Chen, H. Image segmentation using neutrosophic set theory. IEEE Trans. Image Process. 2013, 22, 4379–4388.
3. Kaifi, R.; Kaifi, R. A review of recent advances in brain tumor diagnosis based on AI-based classification. Diagnostics 2023, 13, 3007. Available online: https://doi.org/10.3390/diagnostics13183007 (accessed on 15 January 2025).

4. Khan, S.R.; Sikandar, M.; Almogren, A.; Din, I.U.; Guerrieri, A.; Fortino, G. IoMT-based computational approach for detecting brain tumor. Future Gener. Comput. Syst. 2020, 109, 360–367. https://doi.org/10.1016/j.future.2020.03.054.
5. Khan, M.A.; Ali, S.; Khan, M.H.; Samar, F. Brain tumor segmentation using neutrosophic refined clustering and morphological processing. Comput. Methods Programs Biomed. 2020, 190, 105341. https://doi.org/10.1016/j.cmpb.2020.105341.
6. Kundu, P. Neutrosophic transformation combined with fuzzy clustering for MRI tumor detection. Comput. Methods Programs Biomed. 2018, 154, 103–116.
7. Majumder, D. Neutrosophic-based morphological approach for MRI brain tumor segmentation. Biomed. Signal Process. Control 2016, 27, 34–45.
8. Mohamed, A.; Abd-Elrahman, M.S.; Hefny, H.A. MRI brain tumor segmentation using neutrosophic refined sets. Biocybernetics and Biomedical Engineering 2018, 38, 437–448. https://doi.org/10.1016/j.bbe.2018.01.003.
9. Renugambal, A.; Selva Bhuvaneswari, K. Image segmentation of brain MR images using Otsu's based hybrid WCMFO algorithm. Comput. Mater. Contin. 2020, 64, 681–700. https://doi.org/10.32604/cmc.2020.09519.
10. Sharif, M.; Amin, J.; Raza, M.; Yasmin, M.; Satapathy, S.C. An integrated design of particle swarm optimization (PSO) with fusion of features for detection of brain tumor. Pattern Recognit. Lett. 2020, 129, 150–157. https://doi.org/10.1016/j.patrec.2019.11.017.
11. Smarandache, F. Neutrosophic set a generalization of the intuitionistic fuzzy set. Int. J. Pure Appl. Math. 2005, 24, 287–297.
12. Smarandache, F. Neutrosophic Set—A Generalization of the Intuitionistic Fuzzy Set; University of New Mexico: Albuquerque, NM, USA, 2013. Available online: https://fs.unm.edu/IFS-generalized.pdf (accessed on 15 January 2025).
13. Sofia Jennifer, J.; Sree Sharmila, T. Neutrosophic approach for glaucoma detection in retinal images. Proc. Romanian Acad., Ser. A 2022, 4.
14. Sofia Jennifer, J.; Kalaivani, C. A neutrosophic approach for breast mass detection in digital mammogram images. Neutrosophic Sets Syst. 2024, 73, 1.
15. Villanueva-Meyer, J.E.; Mabray, M.C.; Cha, S. Current clinical brain tumor imaging. Neurosurgery 2017, 81, 397–415. Available online: https://doi.org/10.1093/neuros/nyx103.

Received: Sep 25, 2025. Accepted: March 4, 2026